DSF-36/2006, FERMILAB-PUB-06-478-A

The Signature of Large Scale Structures on the Very High Energy Gamma-Ray Sky

A. Cuoco[1], S. Hannestad[2], T. Haugbølle[2], G. Miele[1], P. D. Serpico[3], H. Tu[2,4]

[1] Dipartimento di Scienze Fisiche, Università di Napoli *Federico II* and INFN Sezione di Napoli, Complesso Universitario di Monte S. Angelo, Via Cinthia, I-80126 Napoli, Italy.

[2] Institut for Fysik og Astronomi, Aarhus Universitet Ny Munkegade, Bygn. 1520 8000 Aarhus Denmark.

[3] Particle Astrophysics Center, Fermi National Accelerator Laboratory, Batavia, IL 60510-0500 USA.

[4] Department of Physics and Astronomy, University of California, Irvine, CA 92697-4575 USA

Abstract. If the diffuse extragalactic gamma ray emission traces the large scale structures of the universe, peculiar anisotropy patterns are expected in the gamma ray sky. In particular, because of the cutoff distance introduced by the absorption of 0.1-10 TeV photons on the infrared/optical background, prominent correlations with the local structures within a range of few hundreds Mpc should be present. We provide detailed predictions of the signal based on the PSCz map of the local universe. We also use mock N-body catalogues complemented with the halo model of structures to study some statistical features of the expected signatures. The results are largely independent from cosmological details, and depend mostly on the index of correlation (or bias) of the sources with respect to the large scale distribution of galaxies. For instance, the predicted signal in the case of a quadratic correlation (as it may happen for a dark matter annihilation contribution to the diffuse gamma flux) differs substantially from a linear correlation case, providing a complementary tool to unveil the nature of the sources of the diffuse gamma ray emission. The chances of the present and future space and ground based observatories to measure these features are discussed.

PACS numbers: 95.85.Pw, 98.70.Vc, 95.35.+d

1. Introduction

Gamma ray astronomy is a flourishing field in astroparticle physics. Results have rapidly accumulated in the last decade or two: after the break-through results of the EGRET satellite, a whole series of Earth-based observatories have developed, both using the imaging air Cherenkov telescopes (ACT like WHIPPLE, HEGRA, CANGAROO, HESS, and MAGIC) or surveying the sky via extensive air showers (EAS detectors, like TIBET, ARGO, and MILAGRO). New projects using all these techniques (the ACTs VERITAS, HESS II, MAGIC II, MACE, the EAS detector HAWC, the satellites AGILE and GLAST) are on the way (for a recent review of the field, see [1]).

At TeV energies, a few dozen sources have been detected mainly by air Cherenkov experiments, most of which are high energy counterparts of MeV-GeV sources in the EGRET catalog. The 0.1–10 TeV range represents one of the "last" photonic windows yet to be explored at large distances. Starting from an energy of about 100 GeV (which we shall refer to as very-high energy, VHE), the absorption of high energy photons onto the extragalactic background light (EBL) via pair-production introduces an energy-loss horizon of the order of a few hundreds Mpc or smaller, well below the size of the observable Universe. This horizon drops down to $\sim$10 kpc at PeV energies, basically precluding deep space astronomy with photons above about 10 TeV. Far from being only a limitation, this phenomenon also allows the use of γ-ray astronomy to probe the EBL, which is otherwise difficult to study directly.

Besides single sources, wide field of view instruments and satellite-based observations are sensitive to diffuse γ-ray emissions. A particularly interesting emission is the extragalactic diffuse γ-ray background (in the following, cosmic gamma background, or CGB). The CGB is a superposition of all unresolved sources emitting γ-rays in the Universe and provides an interesting signature of energetic phenomena over cosmological time-scales. While a clear detection of this background has been reported by the EGRET mission [2], its origin is still uncertain, despite the fact that many models have been proposed. The most likely contribution is the one from unresolved blazars, i.e. beamed population of active galactic nuclei [3], with (probably sub-leading) components from ordinary galaxies [4], clusters of galaxies [5], and gamma ray bursts [6]. However, exotic possibilities like dark matter annihilation have been proposed, that are compatible with existing data and constraints [7, 8, 9, 10]. It is extremely difficult to test such models as long as the only observable is the energy spectrum. Recently, it was proposed to use the peculiar small-scale anisotropy encoded in the MeV-GeV gamma sky to probe dark matter [11] or astrophysical [12, 13] contributions to the CGB. In this work, we further study this topic, with particular emphasis on the large scale anisotropy in the energy range 0.1-10 TeV. The lower part of this range will be probed by the GLAST telescope [14, 15], while the energy window above the TeV is in principle accessible to EAS detectors. Different candidates to explain the CGB predict distinctive large scale features, even when similar energy spectra are expected. This is a consequence of the combined effect of a cutoff distance after which VHE γ can travel

undamped to us, and of the anisotropic distribution of matter in the local universe (i.e., within a few hundred Mpc from us). A similar anisotropy pattern in the the ultra-high energy cosmic ray sky was recently analyzed by some of the authors [16] (see also [17]). The main goal of this paper is to characterize various features of the CGB which may be used for diagnostics at VHE.

We do not attempt here to derive the properties of the CGB from specific astrophysical models, such as blazars (see e.g. [18]) or large-scale structure shocks (see [19, 20, 21]). Instead, we shall consider a phenomenological and parametric approach, analyzing in detail the angular patterns vs. energy for two representative diffuse background models: in the first case, we assume that underlying gamma emitters correlate linearly with overdensities in the large scale structure density field. In the second case, we assume a quadratic correlation. Loosely, one may consider the first case as representing unbiased, unresolved astrophysical sources; the second one may be indicative of a strongly biased astrophysical population of sources, or eventually of dark matter annihilation emission‡, provided it is not dominated by substructures (see [22] for a discussion of this point). Of course, the yet unknown sources of the CGB may have a non-trivial bias and evolution with redshift. To a great extent, additional information on this topic will be provided by the study of the numerous point-like sources that GLAST is expected to resolve. At present, our analysis should be considered as a parametric approach to evaluate the sensitivity to "effective" matter tracing properties and bias of gamma ray sources.

The paper is structured as follows. The parametrization we use for the CGB, based on EGRET data, is summarized in Sec. 2. In Sec. 3 we introduce our treatment of the cosmic large scale structure: a mock catalogue derived from a dark matter N-body simulation and the 3D power spectrum derived from the Halo Model of non-linear clustering [23, 24, 25, 36]. With these tools, we shall argue that in the VHE range, especially at the largest angular scales, the predictions mostly depend on the large scale structure in the local neighborhood of the Universe. We shall then use the PSCz astronomical catalogue as tracer of the real structures in the nearby universe, thus producing maps of the VHE gamma sky (Sec. 4). In Section 5 we analyse the perspectives for detection of these features using the forthcoming satellite GLAST, and for EAS observatories like MILAGRO. In Sec. 6 we summarize our findings, and conclude. In Appendix A we provide some details on the parametrization of the EBL, and on the method we use to propagate gamma rays and calculate attenuation effects. Appendix B reviews some statistical properties of a discrete poisson process on the sphere, relevant for our estimates of the errors of the multipole maps.

‡ Of course, dark matter emission would also have peculiar features in the energy spectrum (e.g. departure from a power-law shape), associated with the particle physics details. They may constitute an important diagnostic tool for detection.

2. The cosmic gamma background

Experimentally, the CGB is the most difficult component of the diffuse emission to study. Indeed, it is not correct to assume that the isotropic component after extracting point-like sources plus the galactic diffuse emission is entirely extragalactic: even in the pole direction, the CGB is comparable to the Galactic contribution. The deduced CGB thus depends on the adopted model of the Galactic foreground. The analysis undertaken to derive the spectrum of the CGB based on EGRET data provided the intensity spectrum [2]

$$I_\gamma(E) = k_0 \left(\frac{E}{0.451\mathrm{GeV}}\right)^{-2.10\pm0.03} , \tag{1}$$

valid from $E \sim 10$ MeV to $E \sim 100$ GeV, where $k_0 = (7.32 \pm 0.34) \times 10^{-6}\mathrm{cm}^{-2}\mathrm{s}^{-1}\mathrm{sr}^{-1}\mathrm{GeV}^{-1}$. Interestingly, it shows a spectral index remarkably close to the average one of γ-ray blazars detected by EGRET, -2.1 ± 0.3 [26]. EGRET experimental points and the best fit curve are shown in Fig. 1.

It is worthwhile to comment that the foreground subtraction remains a delicate issue, as can be appreciated by the reanalysis of the data performed in [27], based on a revised model for the galactic propagation of cosmic rays. The deduced extragalactic spectrum is significantly lowered with respect to Eq. (1) at intermediate energies, while closer to the original result of Eq. (1) at the lowest and highest energy points. Since the removal of the isotropic galactic emission from the diffuse gamma background is an open problem, and we still lack a complete understanding of the sources of the CGB, we shall simply base our following analysis on the extrapolation of the spectrum of Eq. (1) by one to two orders of magnitude. Actually, the anisotropy pattern in the CGB sky itself may help in the foreground removal. Recently, it was proposed to use the cosmological Compton-Getting effect (whose dipole direction and amplitude are basically energy-independent) to discriminate the truly extragalactic fraction from the galactic foreground [28].

When extrapolating the EGRET flux to higher energies attenuation effects must be taken into account. It is well known that the propagation of photons in the EBL is a crucial issue for gamma astronomy in the VHE range. Absorption of VHE photons through pair-production with CMB, infrared or optical photons distorts an initial source spectrum, in particular by steepening its high energy tail. Astronomy of gamma ray emitters like blazars and active galaxies requires then an accurate modelling of the photon propagation and of the background frequency distribution. In Appendix A we provide a detailed description of the model of the EBL used, and of the treatment of absorption effects. For an overview of the knowledge of the EBL we refer the reader to the review [29]. The expression for the flux expected at Earth in a generic cosmology is given by (see e.g. [30, 8])

$$I(E_\gamma, \hat{n}) \propto \int_0^\infty \mathrm{d}z \, \frac{\rho^\alpha(z, \hat{n})\, g[E_\gamma(1+z)]\, e^{-\tau(E_\gamma, z)}}{H(z)\,(1+z)^3} , \tag{2}$$

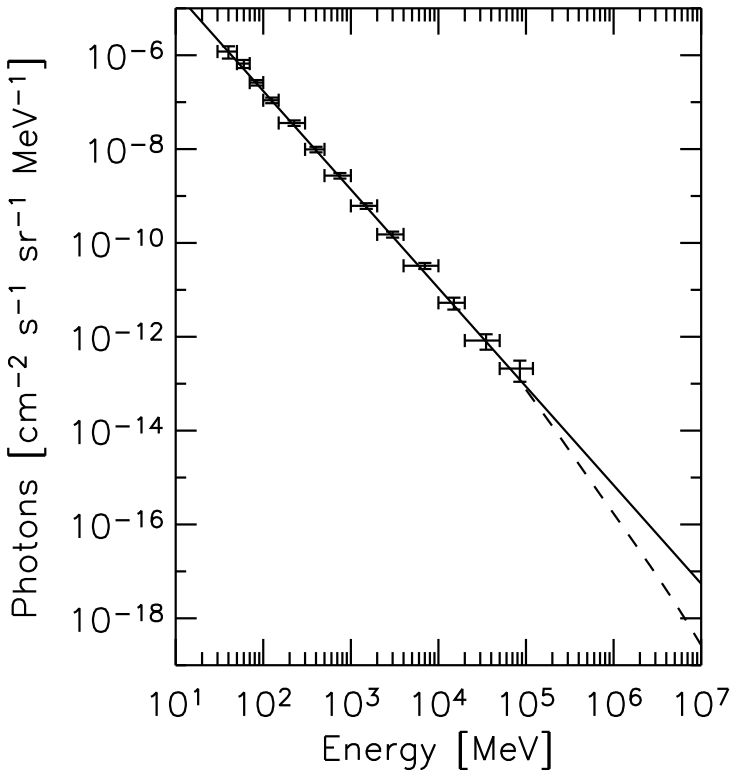

Figure 1. EGRET spectrum from [2] and extrapolation up to 10 TeV. The dashed line shows the expected effect of the pair-production attenuation.

where we assume an universal spectrum for the source, $g(E)$, E_γ is the energy we observe today, $\rho(z, \hat{n})$ is the matter density in the direction $\hat{n}$ at the redshift z, where the sources are assumed to be distributed proportionally to ρ^α. The Hubble parameter is related to the present Hubble expansion rate H_0 through the matter and the cosmological constant energy density as $H(z) = H_0\sqrt{\Omega_M(1+z)^3 + \Omega_\Lambda}$. The quantity $\tau(E_\gamma, z)$ is the optical depth of photons to absorptions via pair production on the EBL (see Appendix A). For most of the following considerations the normalization in the spectrum is irrelevant. Where ever needed (e.g. to estimate the statistics which can be collected by a given experiment) we shall fix the normalization of Eq. (2) so that it matches the EGRET fit of Eq. (1) at 10 GeV.

For most of what follows it is important to realize that, by looking at VHE, most of the dependence on the cosmology, the source evolution, etc. in Eq. (2) cancel out, independently of the index of correlation with density, because of the cutoff at $z \ll 1$ existing for VHE gammas. This important property dramatically reduces the model-dependence of the following considerations. It is also worth commenting that the γ-rays of the CGB constitute only a tiny fraction, f_γ, of the cosmic ray flux. When compared with the flux of cosmic rays around the TeV ($I_{\rm CR} = 2.582 \times 10^{-11}(E/{\rm TeV})^{-2.7}$ cm^{-2} s^{-1} sr^{-1} MeV^{-1} [31]) and neglecting gamma attenuation effects

one gets the upper limit

$$f_\gamma \equiv \frac{I_\gamma}{I_{\rm CR}} \lesssim 2.7 \times 10^{-5} \left(\frac{E}{\rm TeV}\right)^{0.6} . \tag{3}$$

Actually, the attenuation of γ's on the EBL cuts the growth of f_γ, which never exceeds 10^{-5}. Note finally that our extrapolation is consistent with existing observational bounds on f_γ at the TeV scale [31].

3. Tracers of the large scale structure

Since the sources of the CGB are unknown (this is especially true for its high energy component of interest here), to predict the anisotropy pattern in the VHE sky we must start from some assumption on the distribution of the sources. In the following, we shall assume that the sources of the CGB follow the LSS distribution of the matter. Starting from Eq. (2), the integral flux above the energy $E_{\rm cut}$ at Earth is simply written as

$$F(E_{\rm cut}, \hat{n}) \propto \int_0^\infty {\rm d}z \, \frac{\rho^\alpha(z, \hat{n})}{H(z)\,(1+z)^3} W(E_{\rm cut}, z) \,, \tag{4}$$

where we have defined the window function as

$$W(E_{\rm cut}, z) \equiv \int_{E_{\rm cut}}^\infty {\rm d}E \, g[E(1+z)] \, e^{-\tau(E,z)} \,. \tag{5}$$

In the limit where the effective cutoff $z_c \ll 1$, the integrals become almost independent on the cosmology, and the above expressions simplify considerably to

$$W(E_{\rm cut}, z) \simeq \int_{E_{\rm cut}}^\infty {\rm d}E \, g(E) \, e^{-\tau(E,z)} \,, \tag{6}$$

$$F(E_{\rm cut}, \hat{n}) \propto \int {\rm d}z \, \rho^\alpha(z, \hat{n}) \, W(E_{\rm cut}, z) \,, \tag{7}$$

where z is directly proportional to the distance, $r \simeq c\,z/H_0$. In particular we shall assume in the following the power-law $g(E) \propto E^{-2.1}$, which on the theoretical side is consistent with a Fermi-shock acceleration mechanism, and observationally matches both the average spectral index of blazar and the spectra of the CGB measured by EGRET, see Eq. (1).

The size of the horizon is roughly 300 Mpc h^{-1} at 1 TeV (see Appendix A) allowing safely the use of existing astronomical catalogues like PSCz to predict the gamma signal. At lower energy, statistical methods like N-body simulations and the Halo model of structures are in principle required to complement existing catalogues, which are not deep and/or wide enough. We shall describe these tools in the next section and use them to derive the expected statistical properties of the anisotropies at $E < 1$ TeV. These analyses indicate that, at least at large angular scales, most of the non-statistical information contained in the surveys can still be retained, allowing one to use the exiting catalogues for cross-correlation studies even at $E < 1$ TeV.

N-Body Simulations – Our primary tool to compute the statistical properties of the matter density distribution is a N-body catalogue. This offers the advantage compared to observations of being virtually free of most of the bias affecting astronomical

catalogues (no extinction regions, no selection effects, no galaxy morphology and color bias, etc). On the other hand, to obtain reliable results one should carefully consider the types of bias introduced by the simulation, like the algorithm used, the minimum scale resolved, and the physical content and processes treated in the numerical experiment.

We have performed a set of pure dark matter N-body simulations with a standard ΛCDM universe, a periodic box size of 800 $h^{-1}\,$Mpc, and resolutions of 512^3 and 768^3 particles using the GADGET2 code [32, 33]. The initial conditions were computed using second order Lagrangian perturbation theory [34]. Placing the observer at an arbitrary point in the box, we have computed the density on logaritmically spaced spherical shells. A smoothed density field $\rho(z, \hat{n})$ is reconstructed with an adaptive algorithm whose smoothing length varies depending on the local number density of dark matter particles identical to the one used in the GADGET2 code. After obtaining the window functions for different energy cuts, the sky map of the integral gamma ray flux above the cut is calculated by integration along radial lines of sight, considering a source density proportional to ρ or to ρ^2. We have checked that the resolution used in the simulation is sufficient to suppress shot noise from undersampling and other numerical artifacts, by comparing the power spectrum extracted at different resolutions. The resulting maps $F(E_{\rm cut}, \hat{n})$ are obtained on a Healpix grid, facilitating the use of standard tools from CMB physics to compute the final power spectrum and multipole coefficients C_l [35]. For the final analysis we used 2048 shells, with 12×1024^2 pixels on each shell or a density grid with almost 25×10^9 pixels. This makes it possible to reconstruct the power spectrum reliably up to $l = 3071$.

Halo Model – In order to check the results of the N-body simulations, we compare the C_l's obtained in the case of linear correlations with the predictions using the Halo Model [23, 24, 25]. This model is known to provide a fast and efficient semi-analytical recipe for describing the clustering of dark matter halos, and of their evolution. Comprehensive reviews of the model can be found in [36, 37]. Assuming that the gamma emitters follow the distribution of the halos, the angular power spectrum of the adimensional gamma flux anisotropy $[F(E_{\rm cut}, \hat{n}) - \langle F(E_{\rm cut})\rangle] \,/\, \langle F(E_{\rm cut})\rangle$ can be calculated with the 3D matter power spectrum $P(k)$ and its normalization provided by the model. In the flat-sky limit and the Limber approximation, it simply reads

$$C_l = \frac{1}{N_w^2} \int \frac{dr}{r^2}\, W^2(E_{\rm cut}, r)\; P\left(k = \frac{l}{r}, z(r)\right) , \tag{8}$$

where the pre-factor $N_w \equiv \int {\rm d}r\, W(E_{\rm cut}, r)$ represents the contribution from the mean intensity $\langle F(E_{\rm cut})\rangle$.

A comparison of the Halo Model and N-body spectra for various energy cuts is shown in the top panel of Fig. 2. To properly normalize the flux resulting from the N-body catalogue we fix the monopole $C_0 = 4\pi$, where the mean flux is derived by integrating Eq. (4) over the average source density found in the simulation. We see that the agreement is pretty good at $100 \lesssim l \lesssim 1000$, while unsatisfactory at very low and high l. The former disagreement depends on the breakdown of the flat-sky (see e.g. Ref. [38]) and the Limber approximation, while the latter depends on

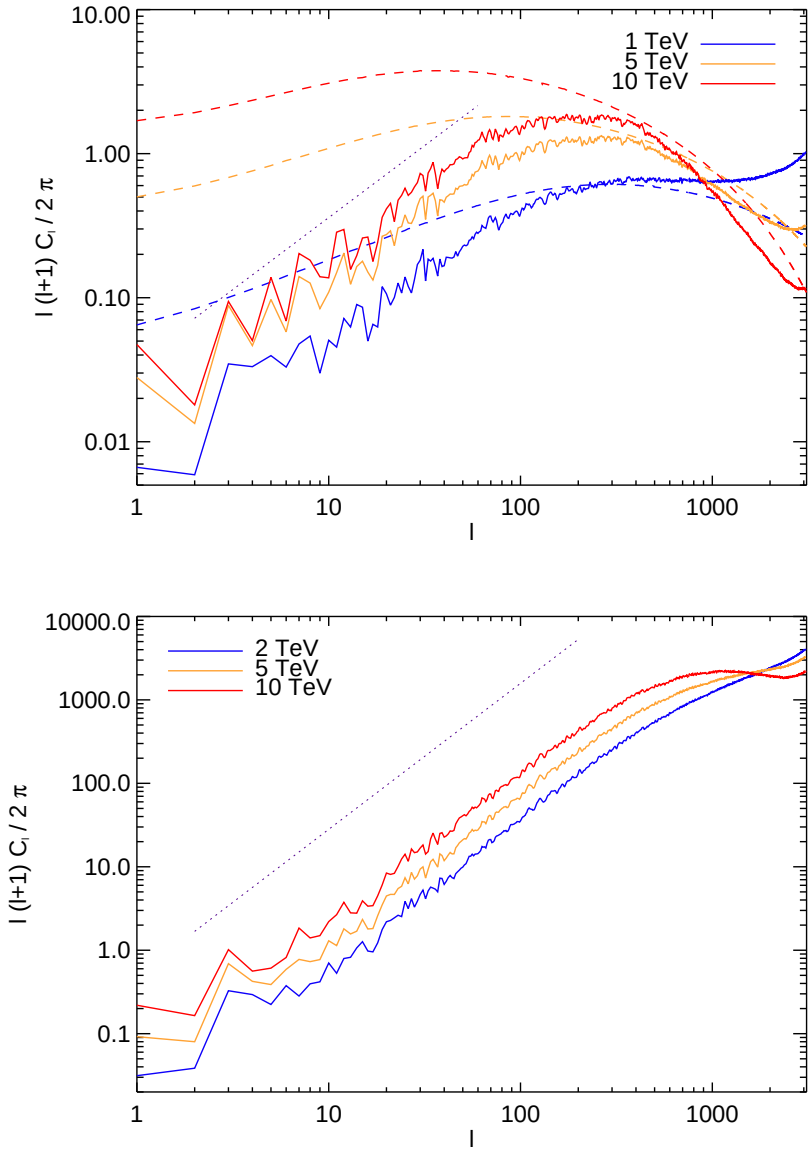

Figure 2. In the top panel we show analytical angular spectra (dashed lines) versus N-body spectra (solid lines) for energy cuts $E_{\rm cut} = 1, 5, 10$ TeV (from bottom to top), in the hypothesis of linear correlation with matter. In the bottom panel we show N-body spectra for a quadratic correlation. In both cases, the dotted line shows the slope of the approximately linear rise of the first multipoles ($l \ll 100$) of the power spectrum. The flux from the N-body simulation is normalized by fixing the monopole: $C_0 = 4\pi$.

the inadequacy of the Halo Model to properly take into account non-linearities for wavenumbers $k \gtrsim 10\ h\,\mathrm{Mpc}^{-1}$. The biggest disagreement is at 10 TeV, for which the window function W is of width $\sim 100\ h^{-1}\,\mathrm{Mpc}$ and the non linear scales are most important. In the N-body catalogue we can only account for the flux coming from distances up to $350\ h^{-1}\,\mathrm{Mpc}$. At relatively low energies ($E_{\rm cut} < 2$ TeV) there are essential

contributions to the flux on small scales/high l from distances further away than that, while negligible contributions to the flux on large scales/low l. At small angular scales and lower energies the simulation also suffers of residual shot noise, seeable in the break in the slope at high l, that makes the comparison biased.

In the lower panel, we present the angular spectrum for the hypothesis of a quadratic correlation with density. Both in the linear and the quadratic case, the three most interesting features are (i) the power law slope at low scales, which is approximately energy independent, as indicated in Fig. 2 by the dotted purple line, (ii) the presence of a peak (deriving from the peak of the 3D matter power spectrum), and (iii) the increasing relative amplitude of the anisotropies with growing energy cut. At relatively large scales, the anisotropies are contributed by the near structures, which are therefore poorly affected by the shrinking of the pair-production energy loss horizon. The isotropic or small-scale varying component of the flux has instead a significant contribution from far objects, which are cutted away at high energies. The main difference between the linear and the quadratic case is clearly in the normalization and the slope of the spectrum. In the latter scenario the intensity of the anisotropies is enhanced, and the slope is steeper. The slope can be estimated even at large scales/low l, and it is a signature of the source correlation with the matter density accessible to observations. For a linear density correlation we find $l(l+1)C_l \propto l$ while for a squared density correlation we find $l(l+1)C_l \propto l^{1.75}$. Also interesting is the prominent shift of the peak to very large l in the quadratic case, although it is unlikely that this feature may be observed experimentally.

We turn now to study how shells at different distances r contribute to the various multipoles. Using the predictions of the Halo Model, in Fig. 3 we plot the integrand $r^{-2}\ W^2(E_{\rm cut}, r)\ P(k = l/r)$ versus r for the two energy cuts $E_{\rm cut}$ =100 GeV and 1 TeV at different l's. Note that even for $E_{\rm cut} = 100$ GeV, the C_l's at $l = 10 - 100$ mostly depend on the contribution from structures within a radius of $\simeq 600\ h^{-1}\,$Mpc. Interestingly, the dominant contribution to the first multipoles at $l = 1 - 10$ comes from within a distance of only $\sim 300\ h^{-1}\,$Mpc. Within such distances astronomical catalogues with a large field of view exist (e.g. the 2MASS and PSCz catalogues), providing the actual distribution of matter in the universe, and not only a statistical information on the density field. Thus, one may aim at the study of the pattern of the first few observables a_{lm}'s or, equivalently, of the anisotropy map smoothed to the appropriate resolution. Note that, the amplitude of matter fluctuation has a measured maximum at a wavenumber (scale) corresponding about to $k = 0.02\ h\,{\rm Mpc}^{-1}$ ($\lambda = 300\ h^{-1}\,$Mpc) [39]. Beyond this distance the low l multipoles start to receive decreasing contributions and converge rapidly to their asymptotic value. This is a well known expectation, although only recently detailed study e.g. of the convergence of the dipole has been performed [40]. Actually, as illustrated in Fig. 3 the presence of the window further accelerate the convergence of the low $l < 10$ sky pattern. This point is further illustrated with the help of the N-body simulation. In Fig. 4 we plot the cumulative contribution to the C_l's in function of the maximum distance used in the catalogue, i.e. derived from Eq. (7) when cutting the integral defining $F(E_{\rm cut}, \hat{n})$ at a distance R. The linear and quadratic

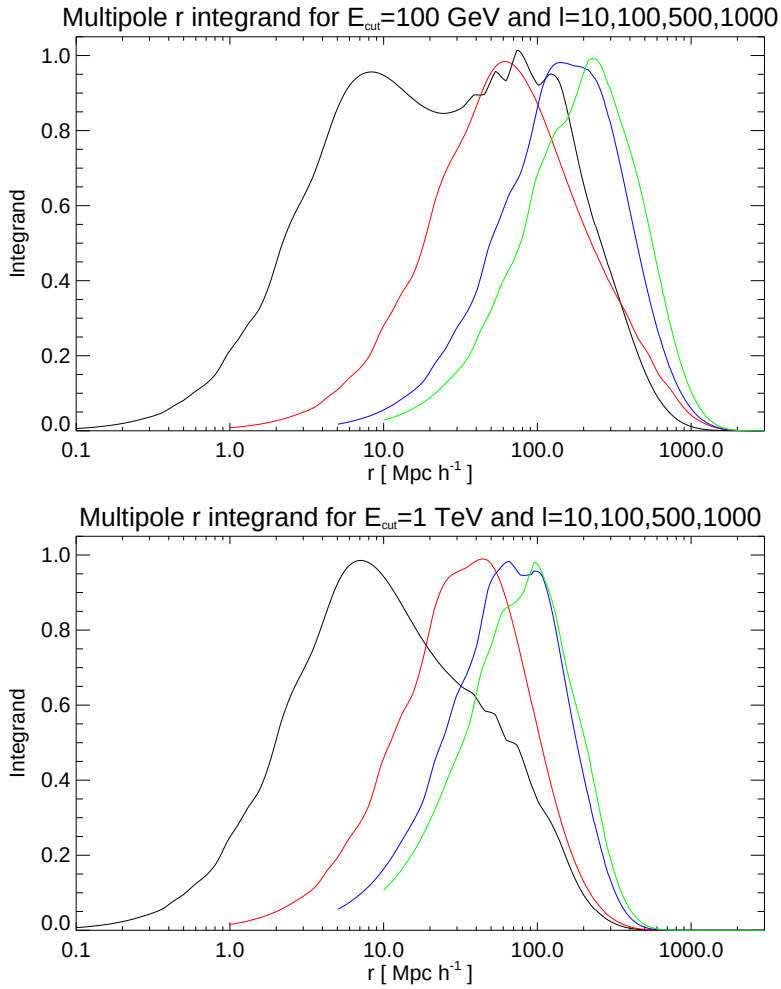

Figure 3. Integrand contributions (linear in $\log r$) for the multipoles $l = 10, 100, 500, 1000$ (respectively, black, red, blue, green) and $E_{\rm cut} = 100$ GeV, 1 TeV. Normalization is arbitrary.

cases are shown, assuming $E_{\rm cut}$=100 GeV (at higher energies, the effect is even more pronounced). Indeed, the simulation confirms that the convergence to the asymptotic value is faster at low l's than at the higher ones. Effectively, for $l \lesssim 10 - 20$ it is meaningful to look for correlations between the gamma sky and known local structures well below the TeV scale. Of course, the argument can be turned around: by masking structures in the nearby sky from the map, the intrinsic low-l multipoles would be largely suppressed, and one may thus access more easily other signatures as the cosmological Compton-Getting dipole [28].

4. Sky maps

In the recent years, modern galaxy surveys like the Sloan Digital Sky Survey [41, 42] have greatly improved our knowledge of the distribution of galaxies at large scales,

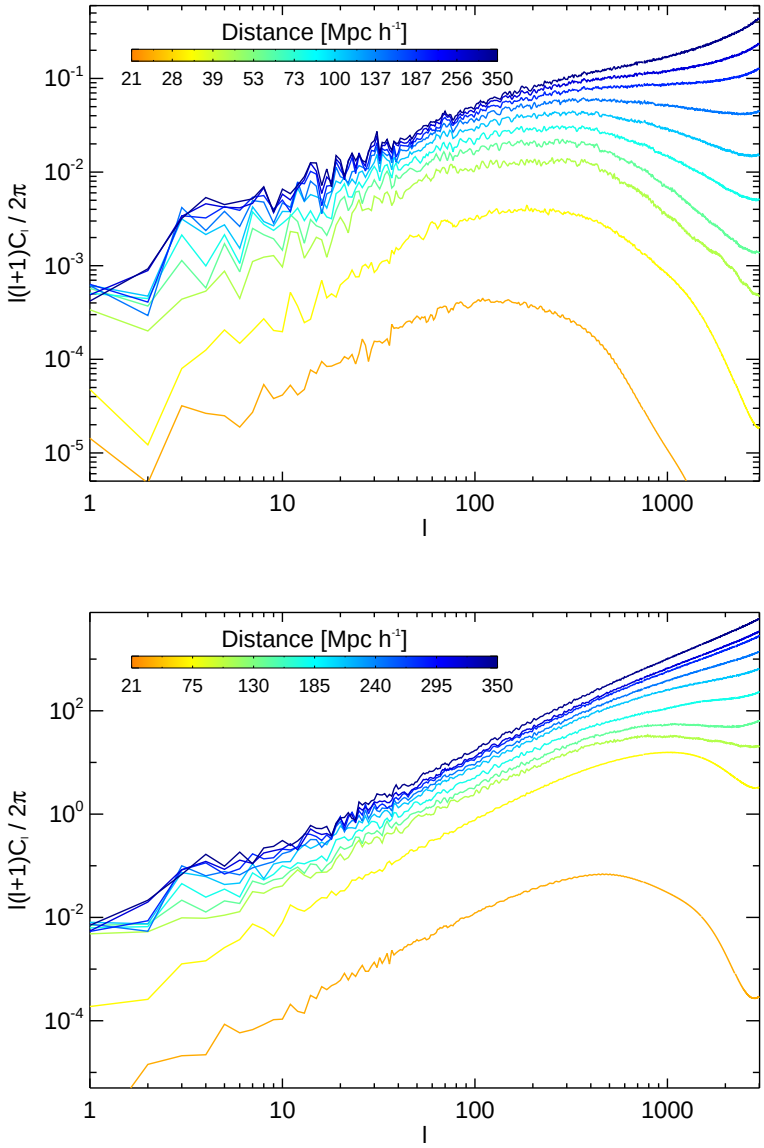

Figure 4. 100 GeV angular spectra when the N-body catalogue is used only until a maximum distance R as function of R. Shown are the linear (top) and quadratic (bottom) density correlation case.

revealing a typical foam-like pattern of "filaments and walls" of galaxies around large cosmological voids. These very high quality data are not well suited for our analysis due to the small fraction of sky surveyed, while we need to perform comparisons with the large sky field of view of GLAST and of EAS instruments. In this respect, a fair compromise is offered by the IRAS PSCz catalogue [43].

The PSCz catalogue contains about 15,000 galaxies and related *spectroscopic* redshifts with a well understood completeness function out to $z \sim 0.1$. In the limit of uniform emission, above $E = 100\,\mathrm{GeV}$ the majority of the CGB flux is expected

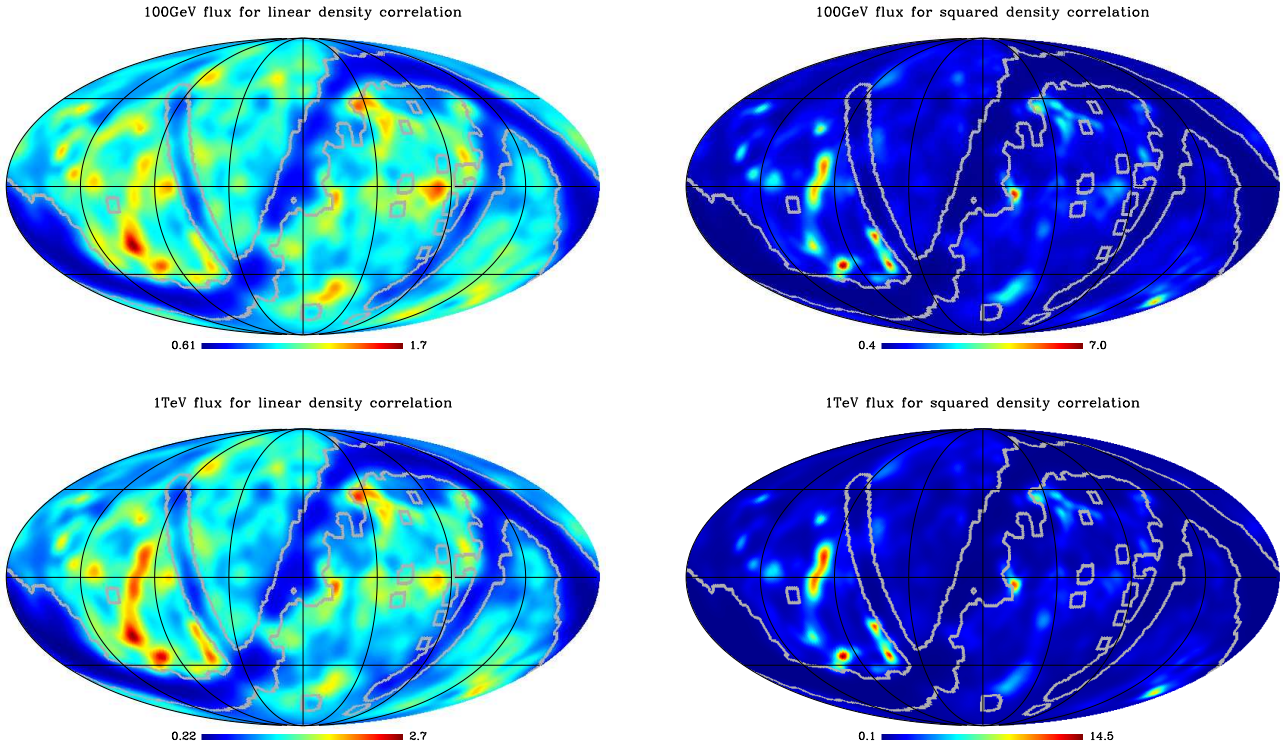

Figure 5. Equatorial density sky maps from the PSCz catalogue for the linear (left) and quadratic (right) density correlation and for $E_{\rm cut} = 100$ GeV and 1 TeV. The color scale is linear and the average flux outside the mask of the PSCz is normalized to 1 so that to represent adimensional maps. The mask of the PSCz survey is enclosed by the thick grey contour.

to come from within this distance. The sky coverage of the catalogue is about 84%; the incompleteness is mainly due to the so called zone of avoidance centered on the galactic plane and caused by the galactic extinction and to a few, narrow stripes which were not observed with enough sensitivity by the IRAS satellite. These regions are excluded from our analysis with the use of the binary mask available with the PSCz catalogue itself. However, the mask region does not represent a major limitation for present analysis, since the galactic emission at low galactic latitudes outshines the CGB anyway, prohibiting any CGB analysis in this region.

We closely follow Ref. [16] for the treatment of the selection effects of the catalogue, parameterized via the selection function $\phi(z)$. Differently from Ref. [16], we do not sum source by source to obtain the final gamma sky map; instead, we use the approach of constructing a smoothed density field $\rho(z, \hat{n})$ through the same adaptive algorithm we employed in the analysis of the N-body simulation. This method has the advantage of efficiently suppressing the intrinsic catalogue shot noise at high redshifts, thus allowing us to use the catalogue sources until $z = 0.1 \simeq 300$ Mpc h^{-1}. We use Eq. (4), while replacing $W(E_{\rm cut}, z) \to W(E_{\rm cut}, z)/\phi(z)$, to take into account selection effects. To study the sensitivity to the bias of the gamma sources with respect to the baryonic density,

Experiment	$A_{\rm eff}$ (cm^2)	$\Omega_{\rm fov}$ (sr)	$f_{\rm sky}$	DC	$g_{\rm cut}$	$h_{\rm cut}$	range
GLAST[46]	10^4	2.4	$f_{\rm m}$	$\sim$90%	$\sim$1	$\sim$.06 f_γ	$E \lesssim$ 0.5-1 TeV
MILAGRO[49]	$\gtrsim 10^7$	~ 2	$\lesssim f_{\rm m} \times 2\pi$	$> 90\%$	0.5	0.08	E $\sim$1–20 TeV
HAWC[50]	$\sim 10^{8.5}$	$\sim$2	$\lesssim f_{\rm m} \times 2\pi$	$> 90\%$	0.5	0.08	E $\sim$0.3–10 TeV

Table 1. The characteristics of the experiments considered in our estimates. The fraction of the sky observable by a given experiment $f_{\rm sky}$ is needed for our estimate of the errors, see Appendix B.

we shall consider both values $\alpha = 1$ and $\alpha = 2$, i.e. a linear and quadratic correlations. The latter is in particular expected for dark-matter annihilation models [44].

In Fig. 5 we plot the resulting maps from the PSCz catalogue in equatorial coordinates for the linear and quadratic density correlation and for $E_{\rm cut} = 100$ GeV and 1 TeV. Let's discuss first the linear case. For the case of the map with $E_{\rm cut} = 100$ GeV, modulo the "hole" due to the mask the pattern is quite isotropic with some hot spots like from the Virgo and Perseus Clusters. Other structures which appear are the Shapley concentration and the Columba cluster (for a key of the local cosmological structures see [16] or [45]). From the color scale can be seen that the anisotropy could be also a factor of 2 in the hot spots, while is generally of the order 10% at larger angular scales as we will show in the following with a multipole decomposition analysis. Given the limited statistics of GLAST at high energies, the TeV map is of interest especially for the EAS gamma detectors like MILAGRO. We see in this case that the nearest structures, forming the Super-galactic Plane, dominate. Of course, from the Northern emisphere (where all the present or planned EAS instruments are located) only the upper part of the map is visible. Here, the Virgo Cluster and the Perseus cluster offer the strongest anisotropy.

For the quadratic case the change is quite evident: the effect of the quadratic correlation is to give more power to the nearest structures (the Virgo and Centaurus cluster) that, in fact, are almost dominating the map with fluctuations exceeding even 10 times the average and appearing almost like point sources. It is instructive to look at the case of Shapley concentration at $z \simeq 0.04$ that gives an important contribution in all the linear cases but almost disappears in the quadratic maps. The anisotropy in the quadratic case is then much more pronounced than the linear case and should be easily detectable.

5. The potential of forthcoming instruments

In order to estimate the chances of detection of the structures previously described by the current or next generation of instruments, one may proceed as follows. First, given the specifics of an experiment (in particular its field of view, effective area and background rejection capability) one calculates the expected number of events and of misidentified cosmic ray background events $(N_\gamma, N_{\rm CR})$ under different assumptions for the $E_{\rm cut}$ and the EBL. The events falling in the mask region must be subtracted from the $(N_\gamma, N_{\rm CR})$

data used for the analysis, so that the incomplete sky coverage is taken into account. One then generates $\mathcal{N}$ samples of N_γ events from the VHE γ map and $N_{\rm CR}$ from an isotropic one. These $\mathcal{N}$ realizations may then be used to perform quantitative statements, like for example the confidence level with which a given instrument is expected to distinguish between the structured sky we predict and an isotropic one, or between linear and quadratic correlation scenarios, or between scenarios characterized by a different model of CIB. This would be essentially the generalization of the approach followed in [16]. Here, however, for the sake of clarity we prefer to develop a simplified analysis in terms of the multipole coefficients, a_{lm}, with an analytic estimate of the expected errors due to shot noise effects (see Appendix B). Performing full Monte Carlo analyses for a few relevant cases we checked that the errors thus estimated basically agree with the ones correctly calculated. In this approach, first we fit the sky maps obtained outside the mask via the harmonic expansion

$$F_{10}(E_{\rm cut},\hat{n}) = \sum_{lm}^{l_{\rm max}=10} a_{lm} Y_{lm}(\hat{n})\,. \tag{9}$$

As a second step, by knowing the statistics and the characteristics of the detector one can estimate the expected errors on the a_{lm} and eventually on the derived coefficients C_l's (see Appendix B for details).

We limit the fit to $l \leq l_{\rm max} = 10$ for several reasons: (i) we have shown that the large scales are mainly sensitive to the local universe, for which our predictions are robust and deterministic; (ii) the lower the l, the higher the signal to noise ratio is, which increases the chances of detection (see below); (iii) the incomplete sky coverage due to the mask is affecting our results, and should be taken into account; however, as long as we restrict the analysis to the large structures (compared to the size of the mask cut) the bias is small. Quantitatively, the method is robust against variations in $l_{\rm max}$ as long as the related angular scale $\theta_{\rm min} = \pi/l_{\rm max}$ is greater than the typical angular extension of the mask cut. More importantly, the purpose of the harmonic analysis is to reliably assess the sensitivity of a given experiment; to this aim a small bias in the a_{lm}'s is acceptable (we do not want to estimate the true a_{lm}'s, but the detectability of them, even of the biased ones). Of course, in the analysis of the real data it will be preferable to directly look for cross correlations with the full maps like the ones in Fig. 5, whose electronic version is available from the authors upon request. Note that a naive a cross-correlation between the gamma sky and the LSS catalogue would not take into account the relevant window function effects we have highlighted in this work.

In the following, we shall consider two kinds of instruments: Satellite-based missions, in particular GLAST [46] (to be launched in the Fall 2007), and extensive air shower experiments like TIBET [47], ARGO [48] (the assembly of which started in October 2000 and is presently being completed), or MILAGRO [49]. The latter experiment is taking science data since 2001, and since 2004 in its outrigger hardware upgrade. In the summer 2007, a transition of MILAGRO to the miniHAWC array is expected to start; this is the first step towards the next generation EAS planned observatories like HAWC [50]. Unfortunately, ACT instruments like HESS or MAGIC

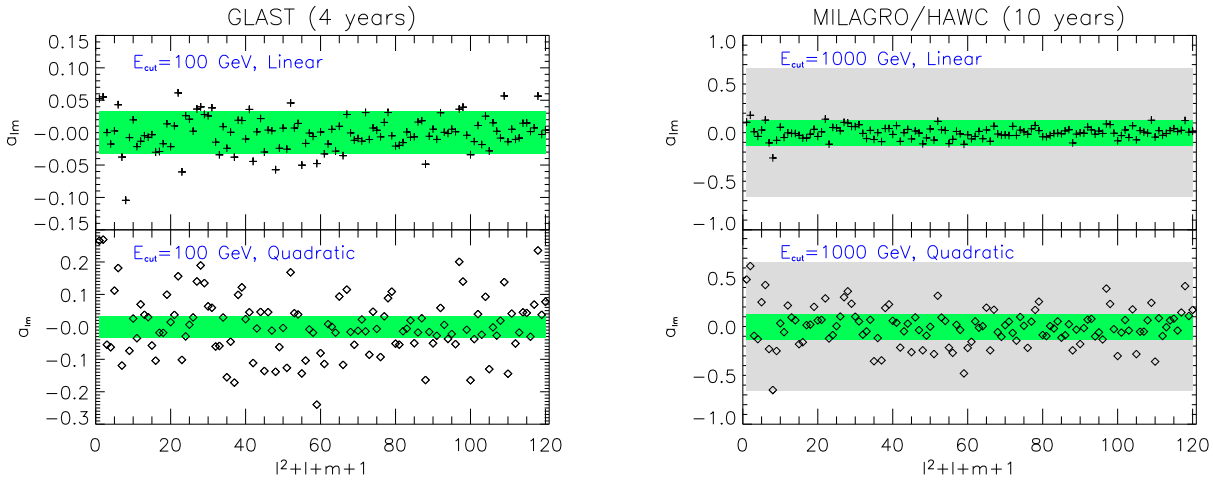

Figure 6. The coefficients a_{lm} up to $l_{\max} = 10$ calculated from the PSCz gamma maps of Fig. 5. The shaded band shows the 1-σ shot noise error given by Eq. (B.6); in the right panel the inner shaded region refers to HAWC, the outer one to MILAGRO. We report the predictions for both the linear and quadratic cases.

are not well suited for such kind of searches, given the small field of view, the low duty cycle, and the relatively high impact of the variability of the instrumental and atmospheric conditions on the rate of diffuse signals.

Denoting by $I_\gamma(E)$ the extrapolated EGRET flux which takes into account attenuations (see Section 2), one can estimate the number of events, N_γ, above the energy E_γ to be collected during the time t as

$$N_\gamma = t \cdot g_{\rm cut} \cdot DC \cdot \Omega_{\rm fov} \cdot f_{\rm m} \int_{E_\gamma}^{\infty} {\rm d}E\, A_{\rm eff}(E) I_\gamma(E)\,, \tag{10}$$

where: DC is the duty-cycle of the instrument; $\Omega_{\rm fov}$ is the solid angle of the field of view; $f_{\rm m} < 1$ is the useful fraction of the sky due to the presence of the galactic mask; $g_{\rm cut}$ is the fraction of γ's passing the actual cuts; $A_{\rm eff}(E)$ is the effective collecting area of the instrument (averaged over the field of view of the instrument). In the following, we shall assume $f_{\rm m} = 0.84$ due to the mask in the PSCz catalogue, but note that future redshift catalogues like 2MRS will have higher $f_{\rm m}$. Eq. (10) assumes a quasi-isotropic γ sky, which may be violated to some extent at the multi-TeV energies of interest for EAS detectors. Even in this case, right ascension anisotropies would not affect the estimate, and only large latitude anisotropies might affect N_γ by a factor of $\mathcal{O}(1)$. This is acceptable enough since we shall only perform a parametric study of the performances of an EAS observatory. Analogously, the CR background can be estimated as

$$N_{\rm CR} = t \cdot h_{\rm cut} \cdot DC \cdot \Omega_{\rm fov} \cdot f_{\rm m} \int_{E_\gamma}^{\infty} {\rm d}E\, A_{\rm eff}(E) I_{\rm CR}(E), \tag{11}$$

where now $h_{\rm cut}$ is the fraction of hadrons passing the cuts. Note that we consider the same area for CRs as for γ's, although a differential performance of the instrument may be taken into account by properly rescaling the factor $h_{\rm cut}$. The typical parameters we shall use are taken from existing literature, and reported in Tab. 1. Note that GLAST is expected to have an excellent background identification, so that only cosmic rays

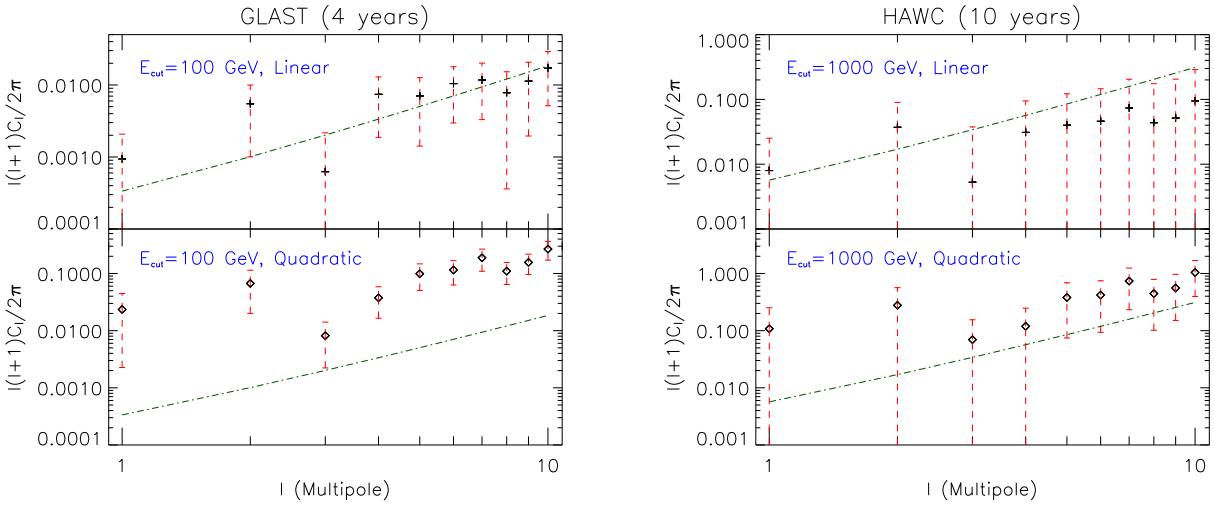

Figure 7. The coefficients C_l up to $l_{\rm max} = 10$ calculated from the PSCz gamma maps of Fig. 5. We shown the level of shot noise [see Eq. (B.5)] expected from four years of GLAST and one decade of HAWC. We report the predictions for both the linear and quadratic cases.

in the amount of $\sim 6\%$ of the gamma flux pass the cuts. On the other hand, EAS experiments have a poor rejection capability (some of them like TIBET [47] have none), which increases typically the gamma content of the diffuse flux by no more than one order of magnitude. Therefore one should keep in mind that even after gamma/hadron separation, the anisotropies of the gamma sky have to be identified against a *quasi*-isotropic background which is $\sim 10^4$ larger than the gamma flux. The ultimate limitation in detecting anisotropies in the gamma sky with EAS observatories is expected to come from the understanding of the intrinsic anisotropy in the CR background. We shall come back to this point in the conclusions.

In Fig. 6 we report the coefficients a_{lm}'s up to $l_{\rm max} = 10$ calculated from the PSCz gamma maps of Fig.5, with the errors estimated according to what reported in Appendix B. The GLAST mission is expected to last 5+5 years (so we plot a realistic 4 years exposure), while EAS instruments have longer run times, so we plot the expectations for a decade of collecting time by MILAGRO, or by the proposed project HAWC. GLAST should be able to detect some structures above 100 GeV at the 2σ level, even if the correlation with matter density is only linear. For a quadratic correlation one expects a more robust detection, and possibly even hints for anisotropies at higher energies§. On the contrary, instruments like MILAGRO may find hints of structures (at the 1 σ level, see gray band in the right panel of Fig. 6) only if correlations are quadratic or in any case strongly biased with overdensities. As a technical remark, note that the performances of MILAGRO above the TeV were estimated by using an effective area $A_{\rm eff}(E_\gamma) \simeq 10^{7.1}\,{\rm cm}^2$ (see e.g. [50]). A proper treatment should take into account the energy-dependence of

§ Our estimate does not include the fraction of the CGB measured by EGRET which may be resolved by GLAST. If this is removed, our predictions should be rescaled accordingly.

the area, and calculate the expected sky maps for MILAGRO weighting accordingly the integral maps. Given the limited chances of this instrument to detect the features we have described, we consider this simple estimate sufficient to illustrate our point. It is worth to stress that for an EAS detector the error on the a_{lm}'s scales as $\sqrt{N_{\rm CR}}/N_\gamma$. Therefore the reduction of the shot-noise error goes like $(t \cdot A_{\rm eff})^{-1/2}$ (both $N_{\rm CR}$ and N_γ grow linearly with $t \cdot A_{\rm eff}$), or equivalently as $\sqrt{h_{\rm cut}}/g_{\rm cut}$: improving the exposure is equally important as improving the gamma/hadron separation capability. A simple inspection of Fig. 6 reveals that for a realistic detection of the features in the VHE sky one would need the improvement in effective area planned to be reached by instruments like HAWC [50] (see inner green band in the right panel of Fig. 6). An instrument like ARGO [48] is expected to have performances in between MILAGRO and HAWC, and may have some chance especially if a significant improvement in hadron rejection can be made. Also, note that due to their altitude HAWC and ARGO have a significant acceptance of sub-TeV events. While the gamma/hadron separation is less efficient at lower energies, the higher statistics may help in revealing these structures.

In Fig. 7 we plot the expectations for GLAST and HAWC in terms of the C_l coefficients. At the large scales we are focusing on cosmic variance makes any detection of the C_l's challenging even when the corresponding a_{lm}'s are easily detectable. This proves the importance of the deterministic nature of the expected anisotropies in the flux.

Since our predictions are shaped by the nearby universe, for a fixed background the absolute value of the detected anisotropy in principle measures the index of the correlation of gamma sources with respect to the matter, as clearly shown by the comparison of the top and lower panels in both Fig. 6 and Fig. 7. On the other hand, a degeneracy exists with the intensity of the infrared background.While an increase in the CIB results in an increased absorption and then in a lower statistics, at the same time the horizon for gammas is shrinking and the intensity of the anisotropy increases too so that the signal to noise ratio remain almost unchanged. In Fig. 8 we compare the two spectra resulting from an increase in the energy cut and an increase in optical depth in order to maintain the same collected statistics or, equivalently, the same noise level C_N. Indeed, at low energies ($E \simeq 100$ GeV) the change in optical depth only slightly reduces the statistics so that the degeneracy is almost perfect. At higher energies ($E \simeq 1$ TeV) the change in statistics is more pronounced and the degeneracy is only partial. A suitable energy cut that gives the same S/N ratio can still be found, while some differences in the multipoles are now visible, although well within typically expected errors. However, both the study of single sources and of the energy spectrum of the CGB should pin down the remaining uncertainty on τ, and the corresponding degeneracy should eventually be broken. GLAST, in particular, will put strong constrains on the intensity of CIB from the study of $\mathcal{O}(10000)$ blazars expected to be detected [55].

Finally, let's note that these estimates are somewhat conservative: summing the power at different l's may favor the detection (see e.g. [13]), and cross-correlating directly with the maps we have produced would eventually rely on the whole information.

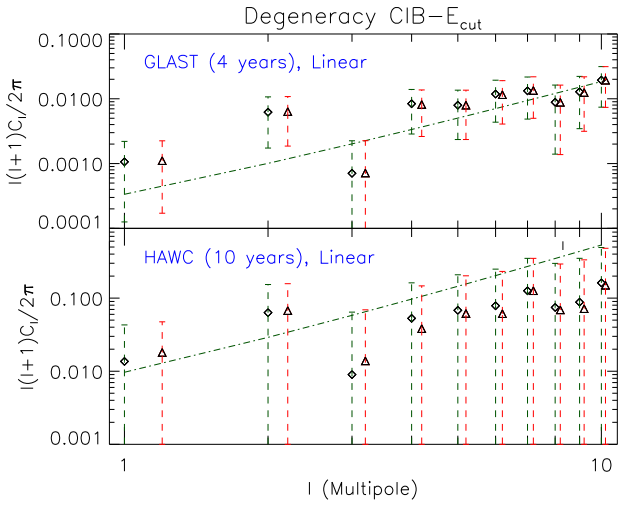

Figure 8. Upper panel: the coefficients C_l up to $l_{\rm max} = 10$ calculated from the PSCz gamma maps of Fig. 5 as in Fig. 7, assuming the fiducial value of the CIB optical depth and an energy cut $E_{\rm cut} = 120$ GeV (diamond symbols, black errors bars) and a CIB value twice the fiducial one (see Appendix A) and $E_{\rm cut} = 100$ GeV (triangle symbols, red errors bars). The value $E_{\rm cut} = 120$ GeV is chosen so that the noise level (dot-dashed line) is the same for the the two CIB values used. Lower panel: same as above for $E_{\rm cut} = 2$ TeV (fiducial CIB value, diamond symbols, black errors bars) and $E_{\rm cut} = 1$ TeV (twice fiducial CIB value, triangle symbols, red errors bars.)

Indeed, to some extent also the information at small scales can be exploited. In particular Fig. 5 shows that the anisotropy expected from small regions of the Virgo cluster and along the Super-Galactic plane is significantly above the average flux. Therefore, once the data on the CGB become available, reassessing the problem with a detailed study will be mandatory.

6. Summary and Conclusions

The universe is pervaded by diffuse backgrounds of low-energy photons, of cosmological origin like the CMB or due to stellar activity, like the optical and infrared background (CIB). This extragalactic background light makes the universe opaque to energetic γ's. The most energetic part of the gamma-ray background (CGB) is thus of primary importance for high energy astroparticle physics, since it acts as a "cosmic calorimeter". Besides telling us about the integrated history of the most powerful astrophysical accelerators of the universe, it may constrain non-standard physics taking place at high energy, even much higher than the GeV−TeV scale. As an example, we remind that the most stringent limits on the decays of superheavy particles coupled at the tree-level *only to neutrinos* come from the observed diffuse extragalactic γ-ray flux [56].

In this work we have studied the anisotropy pattern of the CGB in particular in the very-high energy regime, beyond about 100 GeV. Due to the onset of the pair-production losses of VHE photons on the CIB, most of the flux is coming from local

structures, within $z \lesssim 0.1$. Especially at the largest angular scales, the pattern and *the amplitude* of the anisotropies are almost independent of the source energy spectral shape and of the cosmological model: modulo the magnitude of the CIB, the key parameter in shaping the signature is the degree of the correlation of the gamma-emitters with the known matter density field in the nearby universe (i.e. their bias). For example, unless substructure emission dominates, dark matter annihilation models for the origin of most of the CGB predict a strong (quadratic) correlation of the flux with the matter density, which should clearly manifest in the forthcoming observations. It is interesting to note the nice complementarity of observations made in the few GeV range with the ones in the VHE regime: for example around the GeV the statistics is large and there is no uncertainty introduced by the absorption onto the CIB; on the other hand, the VHE window is promising since, despite the limited statistics, the anisotropies are larger and the predictions are less dependent e.g. on the redshift evolution of the sources. Moreover, the "filtering" of the emission of far sources allows one to use more reliably the deterministic information given by large scale structure catalogues, going beyond merely statistical observables.

Starting from the PSCz astronomical catalogue, we produced maps of the VHE gamma sky and estimated the potential of the satellite mission GLAST or of extensive air shower observatories to detect these features. The GLAST mission should be able to detect a significant correlation of the diffuse gamma-ray emission with the forecast maps presented in this work, providing an important complementary observable to constrain the emission models. This is especially true if an exotic contribution from dark matter annihilation is relevant. Of course, before claiming an unambiguous detection of dark matter in the CGB, detailed particle physics models and a proper foreground analysis are required. Indeed, to some extent strongly biased sources may mimick dark matter-like features. Some early investigation of this issue are however quite promising [22].

EAS experiments are instead limited by the scarce cosmic ray rejection capabilities, and only the next generation of instruments like HAWC (or maybe already ARGO) may have real chances to achieve the needed sensitivity. For EAS experiments, there is a further remark. The Super-Kamiokande experiment has recently detected an anisotropy at the level of few$\times 10^{-4}$ in the cosmic rays around 10 TeV, from a sample of about 2×10^8 muons [52] (MILAGRO has also detected this effect, as mentioned in [53]). At similar or higher energies, the TIBET collaboration has reported the detection of several anisotropies at the $\sim 0.1\%$ level in the cosmic ray flux, probably associated with galactic sources and/or galactic transport [54]. While the exposure needed to reveal the features we have discussed so far is within the reach of the next generation of EAS instruments, even assuming an excellent control over experimental spurious effects, the ultimate limitation in detecting these signatures comes from the understanding of the intrinsic anisotropy in the CR background. Therefore, an efficient gamma/hadron separation is not only necessary to enhance the statistical significance of the point-like or diffuse gamma ray sources observed by EAS instruments, but also to control systematics. In particular, reversing the gamma cut and thus enriching the sample in

hadronic showers may help identifying and removing non-gamma anisotropies.

Acknowledgments

We thank the Danish Centre of Scientific Computing (DCSC) for granting the computer resources used. This work was also supported by the PRIN04 Fisica Astroparticellare of Italian MIUR. PS acknowledges support by the US Department of Energy and by NASA grant NAG5-10842. SH and PS thank the Max-Planck-Institut für Physik in Munich for hospitality and support during the initial phase of this work. TH thanks the DARK Cosmology Centre for hospitality during the course of this work. PS acknowledges the members of the MAGIC group in Munich and of the GLAST group at KIPAC/Stanford, and in particular Daniel Mazin and David Paneque, for useful discussions. HT thanks Manoj Kaplinghat.

Appendix A. Gamma Propagation

Here we report some details on the models used for the extragalactic background light (EBL), and on the technique to account for absorption effects in the propagation of photons. The main component of the EBL is the cosmic microwave background, the spectral number density of which is well known to obey a black-body spectrum

$$n_{\rm CMB}(\epsilon) = \frac{1}{\pi^2\,(\hbar c)^3}\frac{\epsilon^2}{\exp\left(\epsilon/T^0_{\rm CMB}\right)-1} \tag{A.1}$$

where $T^0_{\rm CMB} = 2.73\,{\rm K}{=}2.35{\times}10^{-4}{\rm eV}$ is its present temperature. For the Infrared/Optical Background (CIB), which is the main source of gamma absorption, we use the simple parametrization

$$n_{\rm CIB}(\epsilon) = \begin{cases} 5.42{\times}10^{11}{\rm eV}^{-1}{\rm cm}^{-3}\frac{\epsilon^{3.4}}{\exp(\epsilon/T_F)-1} & \lambda \in 200 \div 2000\,\mu{\rm m}, \\ 7.4{\times}10^{-4}{\rm eV}^{-1}{\rm cm}^{-3}\epsilon^{-2.295} & \lambda \in 6.0 \div 200\,\mu{\rm m}, \\ 7{\times}10^{-3}{\rm eV}^{-1}{\rm cm}^{-3}\frac{e^{-\epsilon}}{\epsilon} & \lambda < 6.0\,\mu{\rm m}, \end{cases} \tag{A.2}$$

where $T_F = 13.6\,{\rm K}$; and the $\lambda - \epsilon$ conversion factor is given by $\lambda(\mu{\rm m}) = 1.24/\epsilon({\rm eV})$. This is a conservative estimate of the CIB consistent with data and constraints reported in [29].

The time evolution of the backgrounds is obtained simply by redshifting, i.e.

$$n(\epsilon, z) = (1+z)^2 n_0\left[\frac{\epsilon}{1+z}\right]. \tag{A.3}$$

This result is exact for the CMB that is a truly primordial background, while for CIB one should in principle perform a simulation of the star formation and dust clustering that produced this background in the recent past. However accurate modelling of this process suggests that most of the background formed in a burst at $z \simeq 4-5$ near the peak of star formation rate, so that for our purposes (propagation till $z \simeq 0.2$) simple redshifting is quite accurate [29].

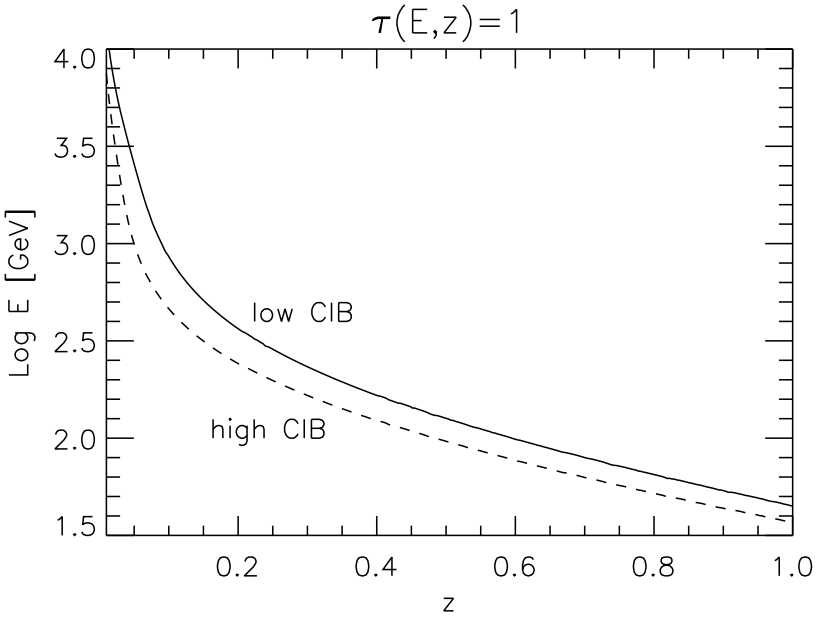

Figure A1. Critical optical depth $\tau = 1$ in function of γ-ray energy and redshift. The low CIB case (dashed line) corresponds to Eq. (A.2), while the high CIB case corresponds to twice that value.

In principle, the interaction of high energy photons with the EBL is a complex process in which the e^-e^+ created through pair production interact again with background photons via inverse Compton scattering producing new high energy γ's. We have developed our own code for calculating the evolution of gamma cascades, along the lines of Ref. [57] (which we refer to for the details, including the general formalism of cascade propagation). Luckily, however, the complicated regime where the cascade of high energy e^+, e^-, and γ has to be followed in details for calculating the final energy distribution is only attained for energies $> 10^{15}$ eV. In the TeV range relevant for gamma astronomy the development of the shower via secondary particle dynamics can be safely neglected, and the observed flux can be calculated by simply considering an energy-dependent depletion factor for the spectrum in addition to the effect of redshifting. Thus, if the spectrum at the source is of the form $g(E)$, the observed spectral shape of the signal will be

$$g(E_\gamma) \propto g[E_\gamma(1+z)]\mathcal{P}(E_\gamma, z), \tag{A.4}$$

where E_γ is the energy we observe today and $\mathcal{P}(E_\gamma, z)$ is the probability for a photon emitted at redshift z to survive without interacting till now, when it reaches us with energy E_γ. This probability is written as

$$\mathcal{P}(E_\gamma, z) \equiv e^{-\tau(E_\gamma, z)}, \tag{A.5}$$

where the optical depth τ is

$$\tau(E_\gamma, z) \equiv \int_0^z \mathrm{d}z' \frac{c}{(1+z')H(z')} \int \mathrm{d}\epsilon\, n(\epsilon, z') \int \mathrm{d}\mu \frac{1-\mu}{2} \sigma_{\mathrm{PP}}(E_\gamma(1+z'), \epsilon, \mu), \tag{A.6}$$

that is the rate of pair production of photons on the EBL integrated over the time during propagating from redshift z to 0. The function $\sigma_{\rm PP}(E, \epsilon, \mu)$ is the theoretically and experimentally well-known pair production cross section of a photon of energy E impinging over a background photon of energy ϵ with a cosinus of the impact angle given by μ. In Fig. A1 we show the derived critical $\tau(E_\gamma, z) = 1$ contour that represents the gamma redshift horizon as a function of the energy. Note that the EBL is known only within a factor of O(2). As we show in Fig. A1 with the case of a doubled optical depth, there is a degeneracy between the energy horizon and the true value of τ. This translates into a degeneracy between the anisotropy pattern and the assumed intensity of the CIB. However, both the study of single sources and of the energy spectrum of the CGB should pin down the remaining uncertainty on this quantity, and the corresponding degeneracy should eventually be broken. Given existing uncertainties, we find a satisfactory agreement of the function τ we computed with more detailed studies including the CIB distribution and evolution from simulations of star and galaxy formation [58].

Appendix B. Summary of the properties of noise

In this Appendix we briefly review the noise properties of a discrete poisson process on the sphere. The main results can be easily obtained analytically and concern the amplitude of the noise variance and the related power spectrum. The map resulting from a random realization of N equally weighted points can be written as $f(\hat{\Omega}) = 4\pi/N \sum_i \delta(\hat{\Omega} - \hat{\Omega}_i)$, normalized to its mean value, so that to be adimensional; then the harmonic expansion coefficients $a_{lm} = \int d\hat{\Omega} f Y_{lm}(\hat{\Omega})$ follow (apart the constant monopole contribution) a gaussian distribution with $\langle a_{lm} \rangle = 0$ and

$$\sigma^2_{a_{lm}} = \langle a^2_{lm} \rangle = \frac{4\pi}{N} \tag{B.1}$$

independent from l, m. From this, the spectrum of the shot noise $C_l = \sum_m |a_{lm}|^2/(2l+1)$ follows a χ^2 distribution with mean

$$\langle C_l \rangle = \frac{4\pi}{N} \tag{B.2}$$

again independent of l, and variance

$$\sigma^2_{C_l} = \langle C^2_l \rangle - \langle C_l \rangle^2 = \left(\frac{4\pi}{N}\right)^2 \frac{2}{2l+1}. \tag{B.3}$$

These results surely hold in the limit of large statistics; however for our applications it is worth testing them also in the limit of very low statistics, say for $N \leq 1000$. We performed a set of Monte Carlo simulations to clarify the issue an found that the simulations and analytic results are in perfect agreement even in the completely unphysical limit of $N = 10$; the analytical results can then be safely used in all the cases of interest.

In general, in addition to the white noise C^N_l, one has a signal C^S_l. Moreover, there is normally incomplete sky coverage, and additional white noise may be present, as in

our case because of the background due to cosmic rays passing the cuts. A generalization of Eq. (B.3) then reads

$$\sigma^2_{C_l} = \frac{2}{(2l+1)f_{\rm sky}}(C_l^S + C_l^N)^2, \tag{B.4}$$

where $f_{\rm sky}$ is the fraction of the sky accessible to the experiment (assumed with uniform acceptance over this region), and the noise spectrum C_l^N (including the cosmic ray background) is given by

$$C_l^N = \frac{4\pi f_{\rm sky}}{N_\gamma}\left[1 + \frac{N_{\rm CR}}{N_\gamma}\right]. \tag{B.5}$$

For the a_{lm}'s, the variance due to the shot-noise plus the background is written as

$$\sigma^2_{a_{lm}} = C_l^N = \frac{4\pi f_{\rm sky}}{N_\gamma}\left(1 + \frac{N_{\rm CR}}{N_\gamma}\right). \tag{B.6}$$

In principle, the complete formulae receive a correction at large l due to the finite angular resolution of the experiment that is easily implemented performing everywhere the substitution $C_l^N \longrightarrow C_l^N \exp(l^2\sigma_b^2/2)$ σ_b being the angular resolution of the experiment. However, since the experimental resolutions are better than a degree, and we limit our considerations to the most prominent signatures at large scales, this correction is unnecessary for our application.

We have used these results in estimating the errors reported in Sec. 5. Note that what is really measured is always the sum signal+noise: the noise is an unavoidable component in any experiment. However, being constant in l, m, the average level of the noise can be fitted and subtracted (this is trivial for deterministic predictions since $\langle a_{lm}^N \rangle = 0$). On the other hand, the error in its determination depends on the sensitivity of the experiment and thus the statistics collected, and on the level of background rejection.

References

[1] R. A. Ong, "The status of VHE gamma-ray astronomy," based on the Rapporteur Talk at ICRC 2005 [astro-ph/0605191].

[2] P. Sreekumar *et al.* [EGRET Collaboration], "EGRET observations of the extragalactic gamma ray emission," Astrophys. J. **494**, 523 (1998) [astro-ph/9709257].

[3] F. W. Stecker and M. H. Salamon, "The Gamma-Ray Background from Blazars: A New Look," Astrophys. J. **464**, 600 (1996) [astro-ph/9601120].

[4] V. Pavlidou and B. D. Fields, "The Guaranteed Gamma-Ray Background," Astrophys. J. **575**, L5 (2002) [astro-ph/0207253].

[5] S. Gabici and P. Blasi, "The gamma ray background from large scale structure formation," Astropart. Phys. **19**, 679 (2003) [astro-ph/0211573].

[6] T. Totani, "Gamma-ray bursts, ultra high energy cosmic rays, and cosmic gamma-ray background," Astropart. Phys. **11**, 451 (1999) [astro-ph/9810207].

[7] L. Bergstrom, J. Edsjo and P. Ullio, "Spectral gamma-ray signatures of cosmological dark matter annihilations," Phys. Rev. Lett. **87**, 251301 (2001) [astro-ph/0105048].

[8] P. Ullio, L. Bergstrom, J. Edsjo and C. G. Lacey, "Cosmological dark matter annihilations into gamma-rays: A closer look," Phys. Rev. D **66**, 123502 (2002) [astro-ph/0207125].

[9] D. Elsaesser and K. Mannheim, "Cosmological gamma ray and neutrino backgrounds due to neutralino dark matter annihilation," Astropart. Phys. **22**, 65 (2004) [astro-ph/0405347].
[10] D. Elsaesser and K. Mannheim, "Supersymmetric dark matter and the extragalactic gamma ray background," Phys. Rev. Lett. **94**, 171302 (2005) [astro-ph/0405235].
[11] S. Ando and E. Komatsu, "Anisotropy of the cosmic gamma-ray background from dark matter annihilation," Phys. Rev. D **73**, 023521 (2006) [astro-ph/0512217].
[12] P. J. H. Zhang and J. F. Beacom, "Angular Correlations of the MeV Cosmic Gamma Ray Background," Astrophys. J. **614**, 37 (2004) [astro-ph/0401351].
[13] S. Ando, E. Komatsu, T. Narumoto and T. Totani, "Angular power spectrum of gamma-ray sources for GLAST: blazars and clusters of galaxies," astro-ph/0610155.
[14] F. W. Stecker and M. H. Salamon, "GLAST and the extragalactic gamma ray background," astro-ph/9909157.
[15] J. E. McEnery, I. V. Moskalenko and J. F. Ormes, "GLAST: Understanding the high energy gamma-ray sky," astro-ph/0406250.
[16] A. Cuoco, R. D. Abrusco, G. Longo, G. Miele and P. D. Serpico, "The footprint of large scale cosmic structure on the ultra-high energy cosmic ray distribution," JCAP **0601**, 009 (2006) [astro-ph/0510765].
[17] A. Cuoco, G. Miele and P. D. Serpico, "First hints of large scale structures in the ultra-high energy sky?," Phys. Rev. D, in press [astro-ph/0610374].
[18] T. Narumoto and T. Totani, "Gamma-Ray Luminosity Function of Blazars and the Cosmic Gamma-Ray Background: Evidence for the Luminosity Dependent Density Evolution," Astrophys. J. **643**, 81 (2006) [astro-ph/0602178].
[19] F. Miniati, "Inter-galactic Shock Acceleration and the Cosmic Gamma-ray Background," Mon. Not. Roy. Astron. Soc. **337** (2002) 199 [astro-ph/0203014].
[20] F. Miniati, "Numerical Modeling of Gamma Radiation from Galaxy Clusters," Mon. Not. Roy. Astron. Soc. **342** (2003) 1009 [astro-ph/0303593].
[21] F. Miniati, S. M. Koushiappas and T. Di Matteo, "Angular Anisotropies in the Cosmic Gamma-ray Background as a Probe of its Origin," astro-ph/0702083.
[22] S. Ando, E. Komatsu, T. Narumoto and T. Totani, "Dark matter annihilation or unresolved astrophysical sources? Anisotropy probe of the origin of cosmic gamma-ray background," astro-ph/0612467.
[23] U. Seljak, "Analytic model for galaxy and dark matter clustering," Mon. Not. Roy. Astron. Soc. **318** (2000) 203 [astro-ph/0001493].
[24] J. A. Peacock and R. E. Smith, "Halo occupation numbers and galaxy bias," Mon. Not. Roy. Astron. Soc. **318** (2000) 1144 [astro-ph/0005010].
[25] C. P. Ma and J. N. Fry, Astrophys. J. 543 (2000) 503, [arXiv:astro-ph/0003343].
[26] J. Chiang et al., Astrophys. J. **452**, 156 (1995).
[27] A. W. Strong, I. V. Moskalenko and O. Reimer, "A new determination of the extragalactic diffuse gamma-ray background from EGRET data," Astrophys. J. **613**, 956 (2004) [astro-ph/0405441].
[28] M. Kachelriess and P. D. Serpico, "The Compton-Getting effect on ultra-high energy cosmic rays of cosmological Phys. Lett. B **640**, 225 (2006) [astro-ph/0605462].
[29] M. G. Hauser and E. Dwek, "The Cosmic Infrared Background: Measurements and Implications s," Ann. Rev. Astron. Astrophys. **39**, 249 (2001) [astro-ph/0105539].
[30] Y. T. Gao, F. W. Stecker and D. B. Cline, "The Lightest Supersymmetric Particle And The Extragalactic Gamma-Ray Background," Astron. Astrophys. **249**, 1 (1991).
[31] F. A. Aharonian *et al.* [HEGRA Collaboration], "Limits on the TeV flux of diffuse gamma rays as measured with the HEGRA air shower array," Astropart. Phys. **17**, 459 (2002) [astro-ph/0109145].
[32] V. Springel, "The cosmological simulation code GADGET-2," Mon. Not. Roy. Astron. Soc. **364** (2005) 1105 [astro-ph/0505010].
[33] V. Springel, N. Yoshida and S. D. M. White, "GADGET: A code for collisionless and gasdynamical

cosmological simulations," New Astron. **6** (2001) 79 [astro-ph/0003162].
[34] M. Crocce, S. Pueblas and R. Scoccimarro, "Transients from Initial Conditions in Cosmological Simulations," astro-ph/0606505.
[35] K. M. Gorski, E. Hivon, A. J. Banday, B. D. Wandelt, F. K. Hansen, M. Reinecke and M. Bartelman, "HEALPix – a Framework for High Resolution Discretization, and Fast Analysis of Data Distributed on the Sphere," Astrophys. J. **622** (2005) 759 [astro-ph/0409513].
[36] A. Cooray and R. Sheth, "Halo models of large scale structure," Phys. Rept. **372** (2002) 1 [astro-ph/0206508].
[37] R. E. Smith *et al.* [The Virgo Consortium Collaboration], "Stable clustering, the halo model and nonlinear cosmological power spectra," Mon. Not. Roy. Astron. Soc. **341** (2003) 1311 [astro-ph/0207664].
[38] W. Hu, "Weak lensing of the CMB: A harmonic approach," Phys. Rev. D **62**, 043007 (2000) [astro-ph/0001303].
[39] M. Tegmark *et al.* [SDSS Collaboration], "The 3D power spectrum of galaxies from the SDSS," Astrophys. J. **606** (2004) 702 [arXiv:astro-ph/0310725].
[40] M. Rowan-Robinson *et al.*, "The IRAS PSCz Dipole," Mon. Not. Roy. Astron. Soc. **314** (2000) 375 [astro-ph/9912223]
[41] York, D. et al. 2000, AJ, 120, 1579
[42] J. K. Adelman-McCarthy *et al.* [SDSS Collaboration], "The Fourth Data Release of the Sloan Digital Sky Survey," astro-ph/0507711.
[43] W. Saunders *et al.*, "The PSCz Catalogue," Mon. Not. Roy. Astron. Soc. **317**, 55 (2000) [astro-ph/0001117].
[44] G. Bertone, D. Hooper and J. Silk, "Particle dark matter: Evidence, candidates and constraints," Phys. Rept. **405**, 279 (2005) [hep-ph/0404175].
[45] P. Erdogdu *et al.*, "Reconstructed Density and Velocity Fields from the 2MASS Redshift Survey," astro-ph/0610005.
[46] See the URL: `http://www-glast.slac.stanford.edu/`
[47] See the URL: `http://www.icrr.u-tokyo.ac.jp/em/`
[48] A. Alolisio et al., "The ARGO-YBJ experiment in Tibet," Nuovo Cim. C24, 739 (2001); Z. Cao, "Status of the ARGO-YBJ experiment," G. Di Sciascio et al. "Selection of the primary cosmic ray light-component by muon detection at high altitude." 29$^{\rm th}$ International Cosmic Ray Conference (ICRC) Pune, India (August 3 - August 10, 2005); I. Di Mitri, at CRIS 2006, Catania, Italy.
[49] J. A. Goodman [Milagro Collaboration], "Recent results from the Milagro gamma ray observatory," Nucl. Phys. Proc. Suppl. **151**, 101 (2006). R. W. Atkins *et al.*, "TeV gamma-ray survey of the northern hemisphere sky using the Milagro Observatory," Astrophys. J. **608**, 680 (2004).
[50] G. Sinnis, A. Smith and J. E. McEnery, "HAWC: A next generation all-sky VHE gamma-ray telescope," astro-ph/0403096. G. Sinnis, "HAWC A Birds Eye View of the Extreme Universe"
[51] F. Halzen and D. Hooper, "Gamma ray astronomy with IceCube," JCAP **0308**, 006 (2003) [astro-ph/0305234].
[52] G. Guillian *et al.* [Super-Kamiokande Collaboration], "Observation of the anisotropy of 10-TeV primary cosmic ray nuclei flux with the Super-Kamiokande-I detector," astro-ph/0508468.
[53] R. W. Atkins *et al.* [The Milagro Collaboration], "Evidence for TeV gamma-ray emission from the galactic plane," Phys. Rev. Lett. **95**, 251103 (2005) [astro-ph/0502303].
[54] M. Amenomori, Journal-ref, Science, V. 3. n. 5798, p. . n. DOI and 1. 1. 1131702 [Tibet AS-gamma Collaboration], "Anisotropy and corotation of galactic cosmic rays," [astro-ph/0610671].
[55] A. Chen, L. C. Reyes and S. Ritz, "Detecting the attenuation of blazar gamma-ray emission by extragalactic background light with GLAST," Astrophys. J. **608** (2004) 686 [astro-ph/0402152].
[56] V. Berezinsky, M. Kachelrießand S. Ostapchenko, "Electroweak jet cascading in the decay of superheavy particles," Phys. Rev. Lett. **89**, 171802 (2002) [hep-ph/0205218].
[57] S. Lee, "On the propagation of extragalactic high-energy cosmic and gamma-rays," Phys. Rev. D **58**, 043004 (1998) [astro-ph/9604098].

[58] F. W. Stecker, M. A. Malkan and S. T. Scully, "Intergalactic photon spectra from the far IR to the UV Lyman limit for $0 < z < 6$ and the optical depth of the universe to high energy gamma-rays," Astrophys. J. **648**, 774 (2006) [astro-ph/0510449]. See also F. W. Stecker, M. A. Malkan and S. T. Scully, "Corrected Table for the Parametric Coefficients for the Optical Depth of the Universe to Gamma-rays at Various Redshifts," astro-ph/0612048.